Mariner 6, 7, and 9 Ultraviolet Spectrometer Experiment: Analysis of Hydrogen Lyman Alpha Data

DONALD E. ANDERSON, JR.

Department of Astro-Geophysics and Laboratory for Atmospheric and Space Physics
University of Colorado, Boulder, Colorado 80302

Four Lyman α airglow measurements of the limb and disc of Mars, made by ultraviolet spectrometers on Mariner 6 and 7 in 1969 and Mariner 9 in 1971, are analyzed to determine the amount and distribution of atomic hydrogen above 80 km. The variation of atomic hydrogen with altitude is calculated by using time-independent chemical diffusion models from 80 to 250 km, and an exospheric model is used above 250 km. By employing radiative transfer theory that includes effects of pure absorption and accounts for temperature variations in the atmosphere a spherical model of the airglow Lyman α emission is used to produce theoretical intensities for comparison with the data. It is found that (1) the exospheric temperature and distribution in 1971 are consistent with those determined in 1969, (2) the vertical optical depth above 80 km was 2.2 in 1969 and 5 in 1971, and (3) the derived atomic hydrogen distribution from 80 to 250 km requires a source of atomic hydrogen above 80 km. Comparison of observed profiles with chemical diffusion models implies a large downward flow of atomic hydrogen at 80 km coupled with a large upward flow of molecular hydrogen.

Analysis of measured Lyman α radiation produced by resonance scattering of the 1216-Å (1^2S-2^2P) solar Lyman α line by planetary atomic hydrogen H is a method of determining the distribution of atomic hydrogen in a planetary atmosphere. Lyman α airglow measurements, together with appropriate radiative transfer and density models, yield the density distribution and temperature of the upper atmosphere. Mariner 6 and 7 ultraviolet spectrometers that flew by Mars in 1969 observed its Lyman α airglow [*Barth et al.*, 1969] and have provided a unique set of data. These are the only Lyman α data available that contain extended bright limb measurements as well as disc measurements of a planetary atmosphere. Bright limb measurements are sensitive to temperature and density at the base of the exosphere or critical level and give reliable estimates of both the amount of hydrogen in the exosphere and the temperature at the critical level [*Anderson and Hord*, 1971]. Disc measurements are less sensitive to temperature and density at the critical level but depend more strongly on the distribution of H below the critical level. Disc data from Mariner 6 and 7 are analyzed separately and in conjunction with the limb data to determine the amount and distribution of H from the critical level down to the altitude where pure absorption of Lyman α photons by carbon dioxide·CO_2 becomes important. Information gained from the Mariner 6 and 7 analysis is applied to Lyman α data from the Mariner 9 ultraviolet spectrometer to determine the density distribution of atomic hydrogen above 80 km on Mars in 1971. Radiative transfer theory required for this analysis was discussed by *Strickland and Anderson* [1973] and *Anderson and Hord* [1971]. Theoretical distributions of atomic hydrogen from 80 to 25,000 km are obtained by solution of the coupled equations of continuity and diffusion below 250 km (the base of the exosphere) and by solution of the collisionless Boltzmann equation above 250 km. Effects of atmospheric chemistry on the distribution of hydrogen below 250 km are included.

MARINER 6 AND 7 DATA ANALYSIS

On July 31 and August 5, 1969, the first observations of the ultraviolet spectrum of the Martian upper atmosphere were made with ultraviolet spectrometers on board the Mariner 6 and 7 spacecraft. The principal emission features were identified and reported in the literature [*Barth et al.*, 1969]. The hydrogen corona was first detected when the closest point of the spectrometer optic axis to Mars R_p was at a planetocentric distance of about 30,000 km [*Barth et al.*, 1971]. As the spacecraft continued to approach Mars, the Lyman α intensity increased to a maximum when the field of view crossed the illuminated limb. Observations were then made of the illuminated disc of Mars. The spacecraft instruments were then redirected to the bright limb, and a second scan of the bright limb and disc of Mars occurred. The observations continued across the evening terminator onto the dark side of Mars, and finally off the dark limb.

A limb crossing is defined as the passing of the optic axis from the upper atmosphere onto the disc. The angle ψ between the optic axis and the sun subtended at the spacecraft was 117° and 124° for the first limb crossings of Mariner 6 and 7, respectively, and 90° for both second limb crossings. The solar zenith angle θ_0 at R_p was 27° and 34° for the first limb crossings of Mariner 6 and 7, respectively, and 0° for both second limb crossings.

The Lyman α data from Mariner 6 and 7 are plotted in Figure 1. Four of the trajectory parameters important for calculating theoretical intensities are also shown: R, the radial distance to the spacecraft R_p, ψ, and θ_0. Important events occurring during encounter with Mars are indicated. Discussion of the Mariner instruments and reduction of data to the form in Figure 1 were given by *Anderson and Hord* [1971].

Each set of data from Mariner 6 and 7 consists of more than 3000 individual Lyman α spectra taken at intervals of $\Delta R_p \approx 20$ km. The spectra were averaged in groups of 31 for $R_p > 10{,}000$ km and in groups of 16 otherwise. These groups were chosen to be small enough so that the altitude variation of the intensity was not affected. One hour of data is plotted for each instrument, ending with the last spectrum received during encounter with Mars. The first data point plotted occurs at $R_p \approx 18{,}000$ km. The vertical scale is based on absolute calibration of the spectrometers [*Pearce et al.*, 1971].

In this analysis the hydrogen density [H] profile of *Anderson and Hord* [1972] is used above 250 km with critical level

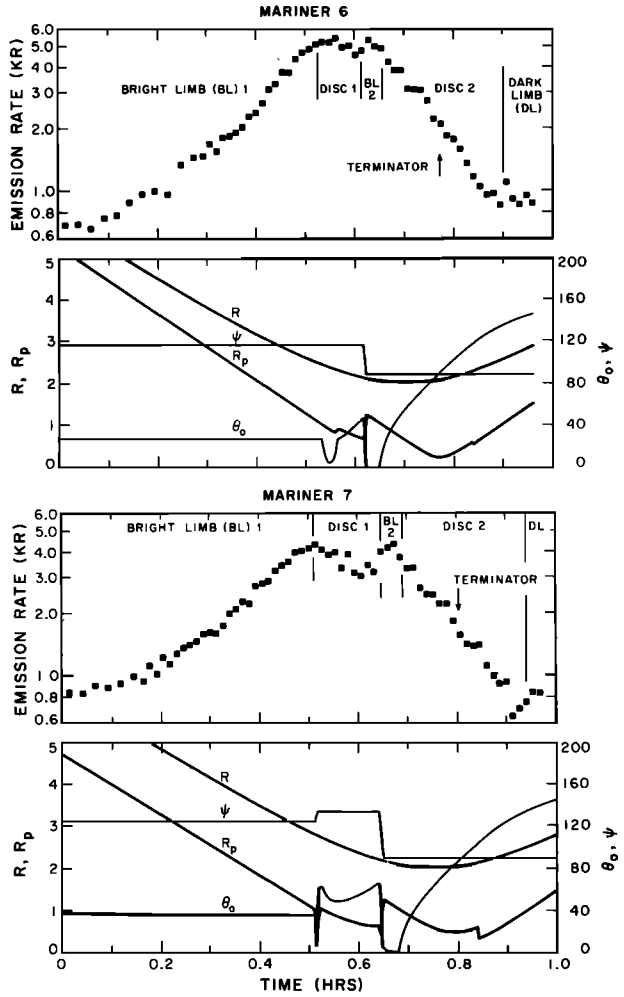

Fig. 1. Mariner 6 and 7 Lyman α limb and disc data together with trajectory parameters.

density $n_c = 2.5 \times 10^4$ cm^{-3} and critical level temperature $T_c = 350°$K. Below 250 km the [H] profiles chosen to model the disc data are shown in Figure 2. The vertical optical depth τ at 80 km associated with models 1–7 is 1.0, 1.2, 1.6, 2.2, 3.4, 5.0, and 15.1, respectively. Model 1 represents diffusive equilibrium, model 2 has approximately infinite scale height below 130 km, models 3–6 have constant scale heights below 130 km, and model 7 represents the solution of the diffusion equation, including the escape flux of hydrogen, down to 80 km. The densities in models 2–6 diverge from the density in model 7 near 130 km, since maximum production of H is assumed to occur near or below this altitude; the flux of hydrogen above this altitude rapidly approaches the escape flux, since there are no chemical losses. Models 1 and 7 are extreme cases, and the correct model should lie between them. Diffusive equilibrium (model 1) implies no escape flux through the region, and in model 7 the maximum production region of H occurs below 80 km.

Theoretical Lyman α emission rates associated with models 1–7 for the Mariner 6 and 7 trajectories are shown in the upper portion of Figures 3 and 4. The intensities in Figures 3 and 4 were calculated by using the spherical isothermal model of *Anderson and Hord* [1971], with pure absorption included. The line center solar Lyman α flux measured by *Bruner and Rense* [1969] was used to determine the absolute value of

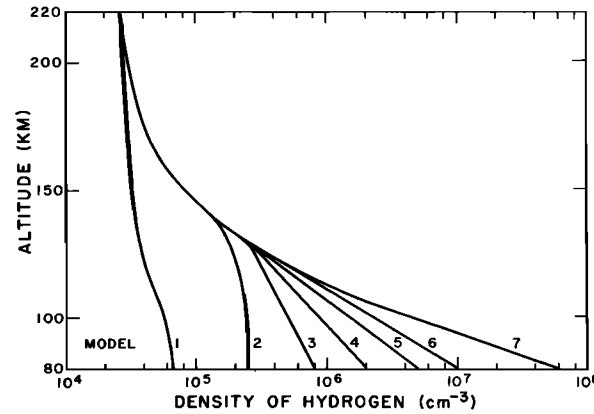

Fig. 2. Atomic hydrogen models used to calculate theoretical intensities. All curves have $n_c = 2.5 \times 10^4$ cm^{-3}.

theoretical intensities. The parameter R_p from Figure 1 is also plotted to indicate changes in the spectrometer line of sight (LOS). Theoretical intensities were calculated once every 15 s ($\Delta R_p \approx 100$ km) when $R_p \simeq 4500$ km. Changes in the theoretical intensities associated with changes in LOS are clearly seen. The gradual spreading in the calculated intensities as the LOS approaches the bright limb is the effect on exospheric intensities of photons scattered by hydrogen below 130 km, since the [H] profile is fixed above this altitude. The convergence of the theoretical profiles on the dark portion of the disc occurs because the hydrogen below 130 km is gradually screened out, first, by the large slant path in H to

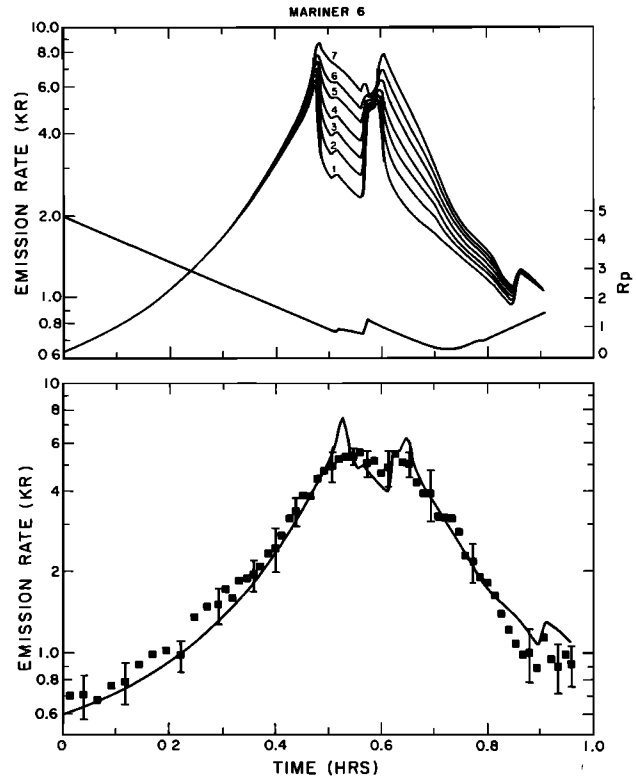

Fig. 3. Theoretical intensities and Mariner 6 data. The upper figure shows theoretical Mariner 6 intensities numbered according to the models in Figure 2. The lower figure shows the best fit to the Mariner 6 data. The solid curve represents model 4 of Figure 2 with $n_c = 2.5 \times 10^4$ cm^{-3} and $T_c = 350°$K, 296 R being added to bright limb theoretical intensities. The R_p is also shown, indicating LOS changes.

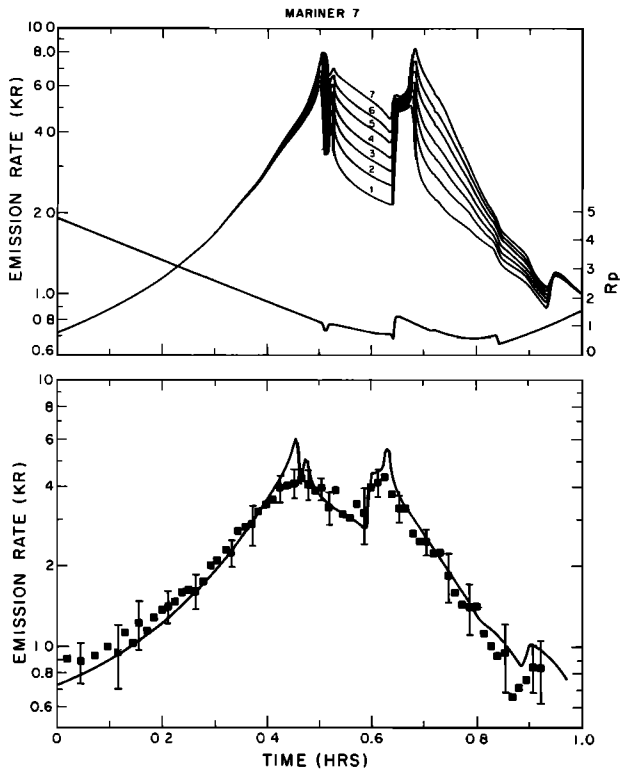

Fig. 4. Theoretical intensities and Mariner 7 data. The upper figure shows theoretical Mariner 7 intensities numbered according to models in Figure 2. The lower figure shows the best fit to the Mariner 7 data. The solid curve represents model 4 of Figure 2 with $n_c = 2.5 \times 10^4$ cm^{-3} and $T_c = 350$°K, 316 R being added to bright limb theoretical intensities. The R_p is also shown, indicating LOS changes.

the sun at low altitudes and second, by the essentially infinite optical depth to the sun in CO_2 below 80 km. For both bright limb crossings of Mariner 6 and 7, 296 R and 316 R sky background were added to the theoretical intensities for Mariner 6 and 7, respectively [*Anderson and Hord*, 1971]. However, no background was added to the dark limb intensities. The theoretical intensity increases at the dark limb because a portion of the photons scattered by hydrogen on the other side of the Mars shadow reach the detector. A varying Doppler temperature will not alter the profiles in Figures 3 and 4 enough to affect the conclusions of this paper. *Strickland and Anderson* [1973] analyzed the temperature effect and obtained a maximum change in intensity of 20%. The maximum occurs for the nadir intensities at the subsolar point and is negligible for the slant paths encountered during the Mariner 6 and 7 flybys.

The best fit to the data was determined by calculation of the minimum value of the rms error and is given by

$$\Delta = \left[\sum w\left(1 - \frac{4\pi\mathcal{I}_c + 4\pi\mathcal{I}_b}{4\pi\mathcal{I}_o + 4\pi\mathcal{I}_b}\right)^2\right]^{1/2}$$

where $4\pi\mathcal{I}_o$, $4\pi\mathcal{I}_c$, and $4\pi\mathcal{I}_b$ are the observed planetary signal, the calculated planetary signal, and the observed sky background emission, respectively, and w is the weight assigned to the total signal $(4\pi\mathcal{I}_o + 4\pi\mathcal{I}_b)$ at a specific time. The term $4\pi\mathcal{I}$ is the intensity in rayleighs or kilorayleighs and is defined so that an apparent column emission rate $4\pi\mathcal{I} = 1$ R is equivalent to an intensity $\mathcal{I} = 10^6/4\pi$ photons cm^{-2} s^{-1} sr^{-1}. The rms error of the fits to the entire set of Mariner 6 and 7 data is plotted in Figure 5 as a function of optical depth at 80 km for the respective models. The rms error was also determined for the portion of the data labeled disc 2. In all four cases, model 4 ($\tau = 2.2$) of Figure 2 gives the best fit to the data. The best fits were determined by allowing each model intensity profile to shift vertically until the rms error was a minimum. Theoretical intensities for the best fits to Mariner 6 and 7 are shown in Figures 3 and 4. The sky background has not been added to the theoretical dark limb profiles because better fits are obtained without the background. Its absence in the data may be due to a narrow sky background line profile: in this case, only about 15% (~50 R) of the emission would reach the detector, since the slant optical depth along the line of sight is ~3. Alternatively, the temperature in the shadow region may be less than that in the sunlit portion of the atmosphere, and the density higher. This situation leads to a larger slant optical depth and greater attenuation of the planetary signal coming from the other side of the Mars occultation cylinder.

Mariner 9 Data Analysis

Mariner 9 was successfully inserted into orbit around Mars on November 14, 1971. The Mariner 9 ultraviolet spectrometer measured the upper atmosphere airglow of Mars for 120 days [*Barth et al.*, 1972*a*; *Barth et al.*, 1972*b*]. The Mariner 9 spectrometer is similar to the Mariner 6 and 7 spectrometers. Orbits 96 and 98 have been chosen for comparison with Mariner 6 and 7. The start of these orbits occurred on December 31, 1971, and January 1, 1972, respectively. The ultraviolet spectrometer scanned the bright disc and limb of Mars for a period of about 1 hour during each orbit. Data for these periods are analyzed here. The values of ψ for orbits 96 and 98 were fixed at 123° and 139°, respectively. In general, ψ was not fixed, but during a few orbits the spacecraft was programed to maintain a constant value of ψ.

The Lyman α data for orbits 96 and 98 are plotted as a function of time in Figure 6. Reduction of the data to this form is identical to the Mariner 6 and 7 data analysis. Each data point represents an average of 15 spectra. The [H] distribution of *Anderson and Hord* [1972] is again used above 250 km with $n_c = 2.5 \times 10^4$ cm^{-3}, since extended limb observations were not obtained in 1971. From analysis of Mariner 9 CO Cameron band intensity profiles, *Stewart et al.* [1972] found $T_c = 325$°K. This agrees well with the temperature deduced in 1969 from measurements of Lyman α by *Anderson*

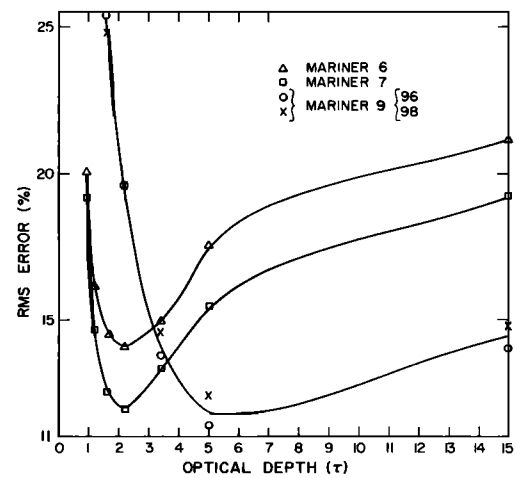

Fig. 5. Distribution of rms errors when the best models at each optical depth are fitted to the Mariner 6, 7, and 9 data.

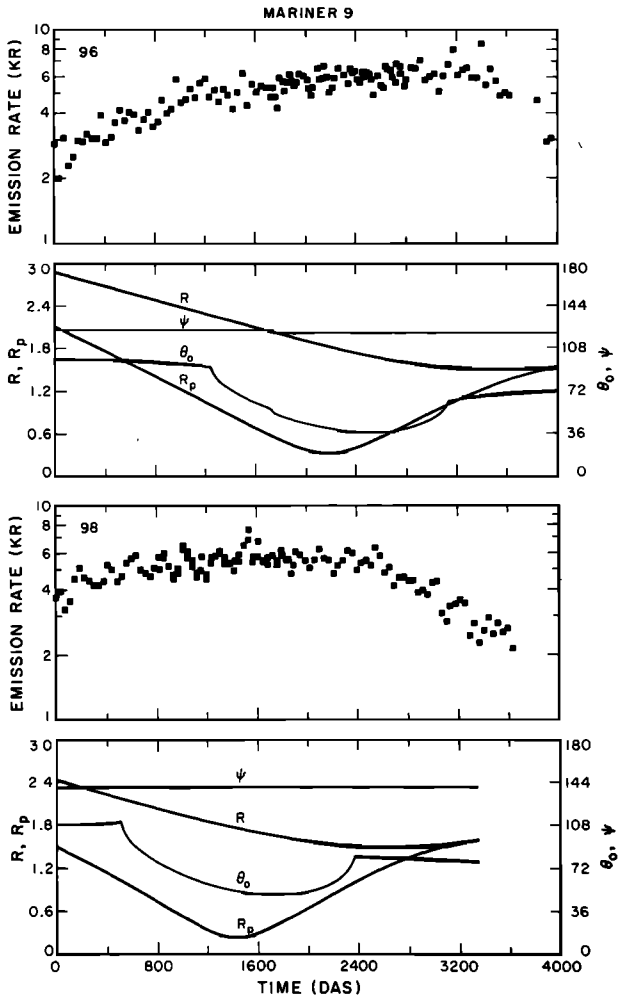

Fig. 6. Mariner 9 Lyman α limb and disc data for orbits 96 and 98 together with trajectory parameters. Time is in spacecraft DAS units, where 1 DAS = 1.2 s.

and Hord [1971] and airglow analysis by *Stewart* [1972]. Below 250 km the [H] profiles are as shown in Figure 2.

Theoretical intensities are shown in Figure 7 for orbits 96 and 98 and have a 300-R background added to the limb intensities, consistent with Ogo 5 measurements of the sky background [*Thomas and Krassa*, 1971]. Intensities were calculated once every 38 s ($\Delta R_p \approx 100$ km). The solar flux of *Bruner and Rense* [1969] was again used in calculating theoretical intensities. The best fits to the data for orbits 96 and 98 for limb and disc spectra are shown in Figure 5. The rms error was also determined for disc data only. Model 6 ($\tau = 5$) of Figure 2 gives the best fit to the data in all four cases.

Solar Flux–Absolute Calibration

The vertical optical depths of 2.2 for Mariner 6 and 7 and of 5 for Mariner 9 were obtained by fitting the shape of the observed intensity profiles and are independent of absolute calibration and solar flux measurement. The magnitude of the observed intensities was based on the absolute calibrations of the spectrometers. The magnitude of the theoretical intensity was determined by using the line center solar flux of *Bruner and Rense* [1969]. These intensities were then shifted vertically with respect to the data until a best fit was obtained at each of the model optical depths. It was found that the factors by which the theoretical intensities must be multiplied to give the best agreement with the observed signals were 0.85, 1.0, and 1.2 for Mariner 6, 7, and 9, respectively. These factors represent the combined errors in absolute calibration of the spectrometers, in determination of τ, and in solar flux measurements. Comparison of Mariner 6 and 9 sky background measurements with Ogo 5 sky background measurements shows that the absolute calibrations of Mariner 6 and 9 ultraviolet spectrometers differ by 43 ± 20% [*Bohlin*, 1973]. Mariner 6 Lyman α intensities should be scaled by 1.43 to agree with Mariner 9 intensities. *Barth et al.* [1972*b*] found that Lyman α intensities were larger in 1971 than in 1969. The 1304-Å radiation from Mars produced by resonance scattering of the solar 1304-Å line was 20 to 30% higher in 1971 [*Strickland et al.*, 1972]. The Mariner 9 data presented here are consistent with these results.

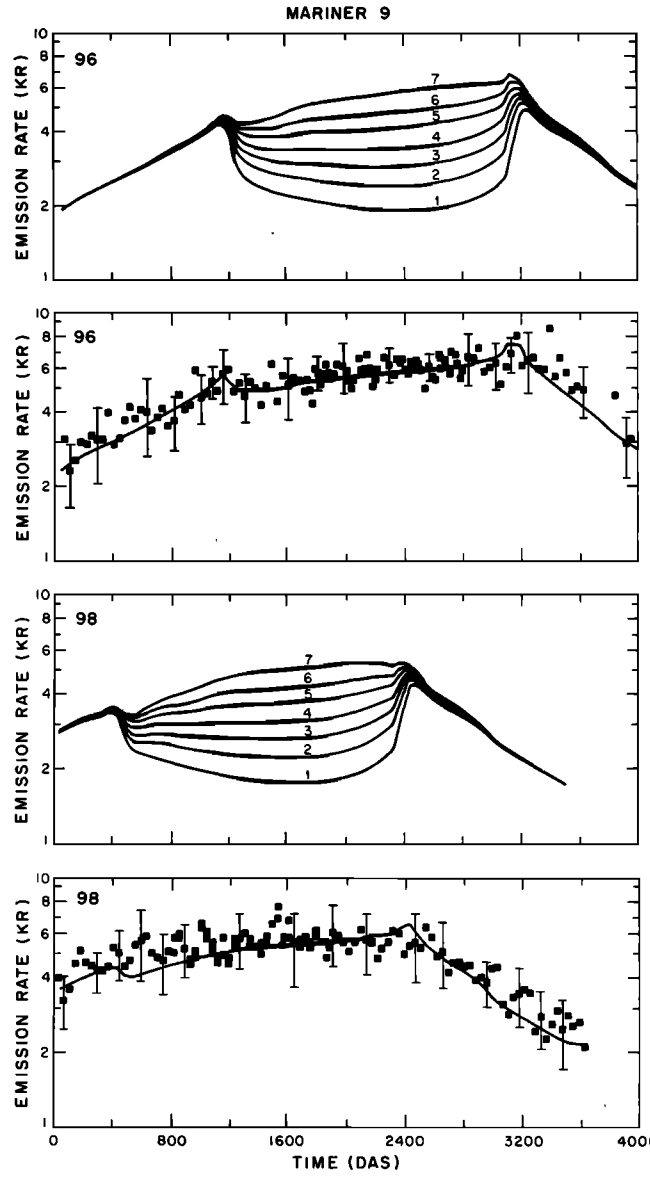

Fig. 7. Mariner 9 theoretical intensities and best fit to data for orbits 96 and 98. The upper pair of figures refer to orbit 96, and the lower pair refer to orbit 98. Theoretical curves are numbered according to models in Figure 2. The solid curves plotted with data represent best fit to Mariner 9, orbits 96 and 98, with $n_c = 2.5 \times 10^4$ cm^{-3} and $T_c = 350$°K, and model 6 of Figure 2, 300 R being added to theoretical limb intensities.

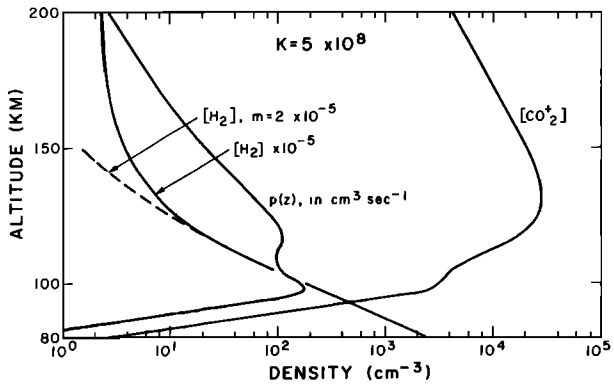

Fig. 8. The $[CO_2^+]$ profile calculated with measured electron density and 1% atomic oxygen at 135 km. The volume production rate $p(z)$, calculated by using the $[H_2]$ profile, is also shown. The dashed curve is the $[H_2]$ profile for the constant mixing ratio of H_2.

Error Analysis

Mariner 6 and 7 disc data analysis shows that a broad minimum in rms error is centered near model 4. Models 3–6 lie within approximately 1% of the minimum rms value. When limb data are included in the analysis, the minimum is deeper, and as is shown in Figure 5, model 6 no longer produces a satisfactory fit. Models 3–5 cover the range of acceptable fits, and thus in 1969 on Mars, $\tau = 2.2\ (+1.2, -0.6)$. The larger rms error in the limb and disc Mariner 6 data relative to the Mariner 7 data arises because the same values of n_c and T_c were used for Mariner 6, 7, and 9. *Anderson and Hord* [1971] found $n_c = 3.0 \times 10^4$ cm^{-3} for Mariner 6 and 2.5×10^4 cm^{-3} for Mariner 7 by using limb data. Thus use of the smaller value of n_c for Mariner 6 produces a larger error.

The Mariner 9 analysis is identical to the Mariner 6 and 7 analysis. The best fit for Mariner 9 predicts $\tau = 5.0$ (model 6). When the error is estimated in the same manner as it was for Mariner 6 and 7, the value for τ is 5.0 (+5, −1). The larger positive error bar reflects the relative insensitivity of the intensity profile as τ gets larger. This is true for Mariner 6 and 7 also, but to a lesser extent, because the shape changes more rapidly as a function of τ at smaller optical depths. It is not possible to measure small changes in the shape of the lower atmosphere distribution as long as the vertical optical depth remains the same.

The utility of using limb and disc data together is that the relative change of theoretical signal as the instrument scans from the limb onto the disc must be consistent with the data. Thus not only the shape of the disc profile but the relative change in the limb-to-disc intensity can be used to determine the best fit to the data. This explains the narrow rms minimum of limb plus disc data relative to disc data only.

Discussion

Chemical diffusion models are now used to suggest physical processes that may explain the observed optical depths. The volume production rate $p(z)$ of H and the molecular hydrogen H_2 density distribution are estimated.

It is assumed that the reaction

$$H_2 + CO_2^+ \rightarrow CO_2H^+ + H \qquad (1)$$

and the reaction following it,

$$CO_2H^+ + e \rightarrow CO_2 + H \qquad (2)$$

are the only chemical sources of H above 80 km and that there are no chemical sinks above 80 km. It is also assumed that $[CO_2H^+]$ is determined by these two reactions. The volume production rate is then

$$p(z) = 2k_1[H_2][CO_2^+] \qquad (3)$$

where $k_1 = 1.4 \times 10^{-9}$ cm^{-3} s^{-1} [*Hunten and McElroy*, 1970].

The $[CO_2^+]$ distribution used is shown in Figure 8 and is calculated above 97 km with the measured electron density and a model atmosphere containing 1% atomic oxygen at 135 km [*Barth et al.*, 1972*b*]. This yields an ionosphere with 30% CO_2^+ and 70% O_2^+. These percentages vary with the amount of O assumed, but $[CO_2^+]$ should not vary by more than a factor of 2. Below 97 km the profile is calculated, a 2.5-km scale height of CO_2^+ being assumed. The eddy diffusion coefficient K used in this discussion is 5×10^8 cm^2 s^{-1} [*McElroy and McConnell*, 1971].

The calculations were perfo.med by using the known values of $n_c(H)$ and $\varphi_c(H)$ at 250 km. The $[CO_2^+]$ distribution was also taken as known, as well as the value of K. The magnitude of the $[H_2]$ distribution above 80 km was then allowed to vary until a satisfactory fit was obtained to model 4. To fit model 6, $n_c(H)$, and therefore $\varphi_c(H)$, was allowed to vary until a best fit was obtained. The assumption was made that $p(z)$ and K were the same above 80 km in 1969 and 1971.

The altitude profiles of $p(z)$ and $[H_2]$ for $n_c(H_2) = 2 \times 10^5$ cm^{-3} are shown in Figure 8. The dashed portion of the $[H_2]$ profile represents a constant mixing ratio $m = [H_2]/[CO_2]$, equal to 2×10^{-5}. The solid curve is the iterated solution of the coupled equations of continuity and diffusion [*Colegrove et al.*, 1966] and is the profile used in calculation of $p(z)$.

Models 4 and 6 of Figure 2 are plotted in Figure 9, together with chemical diffusion solutions that approximate these profiles and give nearly the same optical depths above 80 km. These solutions were calculated by using a thermal diffusion factor equal to −0.25, $p(z)$ in Figure 8, and $T_c = 350$°K. The values of n_c are 2.5×10^4 cm^{-3} and 3.0×10^4 cm^{-3} and of φ_c are 1.4×10^8 cm^{-2} s^{-1} and 1.7×10^8 cm^{-2} s^{-1} for solutions approximating models 4 and 6, respectively. The flux profile $\varphi(z)$ of H calculated by using $p(z)$ in Figure 8 and $n_c = 2.5 \times 10^4$ cm^{-3}, is shown in Figure 10 together with the H_2 flux profile.

Hunten and McElroy [1970] suggested that the $[H_2]$ profile should remain unchanged over a time scale of $\sim 10^8$ years. The $[CO_2^+]$ profile may change if either the electron density or [O] changes. The [O] profile appears to be approximately the

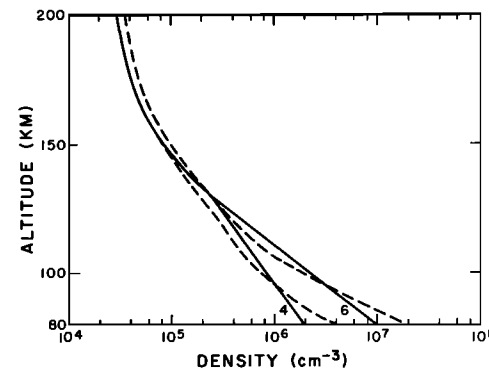

Fig. 9. The solid curves labeled 4 and 6 represent models from Figure 2 that fit Mariner 6 and 7 and Mariner 9 data, respectively. The dashed curves are chemical diffusion models approximating these models.

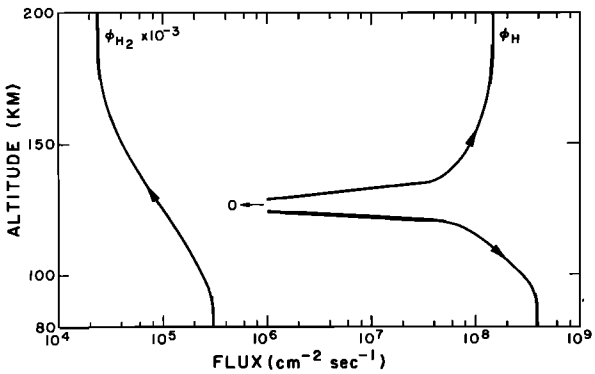

Fig. 10. Flux of H and H_2 calculated by using $p(z)$ of Figure 8 and escape flux of H equal to 1.4×10^8 cm^{-2} s^{-1}.

same in 1971, although daily variations were observed [*Strickland et al.*, 1973]. The electron density profiles are approximately the same at the same pressure level in the atmosphere in 1969 and in 1971 [*Kliore et al.*, 1972]. Below 100 km the electron density profile is not well known. It has been assumed here that the $[CO_2^+]$ profile falls off very rapidly below 100 km with a scale height of 2.5 km. If the scale height is doubled below 100 km, the $[CO_2^+]$ density, and thus $p(z)$, is increased by ~30 times at 80 km. However, this result produces a change of less than a factor of 2 in the H density at 80 km. Thus it is reasonable to assume that $p(z)$ is the same in 1969 and 1971.

In the chemical diffusion model assumed here a change in the flux of H in the region 80–250 km produces the desired change in optical depth. A smaller downward flux of H in 1971 leads to an increase in τ above 80 km. A more stable lower atmosphere, and thus a smaller average value of K below 80 km, reduces the downward flux. Reduction of the sink of H below 80 km produces a similar effect. The difference between solutions in Figure 8 is produced by a change of 20% in the downward flux of H at 80 km. A 20% reduction increases [H] at 80 km by 5 times and at the critical level by 20% if $p(z)$ and K remain unchanged. If the density of H at the surface is ~10^8 cm^{-3}, the scale height is ~10 km, and the sink of H is eliminated, then the time required to increase the amount of H below 80 km by a factor of 5 is ~10 days.

During the Mars global dust storm that lasted past orbit 120 of Mariner 9, *Kliore et al.* [1972] measured isothermal temperature profiles between 0 and 20 km. They suggested that this observation was caused by dust suspended in the atmosphere and that dust was present to an altitude of at least 15–20 km. The isothermal profile may lead to a more stable lower atmosphere. The extinction of ultraviolet radiation by the dust may also alter the hydrogen chemistry in the near-surface region [*Hunten and McElroy*, 1970], the sink of H thus being reduced.

Summary

Disc and limb measurements of Mars Lyman α airglow made by ultraviolet spectrometers on Mariner 6, 7, and 9 have been analyzed. The most significant result of this analysis is the determination of the values of the vertical optical depth of atomic hydrogen above 80 km on Mars in 1969 and in 1971. The values of τ were 2.2 in 1969 and 5 in 1971. The approximate distribution of atomic hydrogen above 80 km was also determined. Analysis of Mariner 9 limb intensities shows that the exospheric distribution in 1971 is consistent with that found in 1969.

Comparison of chemical diffusion models with the observed profiles shows that (1) the observed [H] profiles require a source of H above 80 km, (2) the implied mixing ratio of H_2 is $\sim 2 \times 10^{-5}$, and (3) the difference between the optical depth in 1969 and that in 1971 is explained by a 20% reduction in the downward flow of H at 80 km in 1971.

This study shows that with combined limb and disc measurements of Lyman α radiation from a planetary atmosphere it is possible, for moderate optical depths, to determine the amount and distribution of atomic hydrogen down to the level where pure absorption becomes important.

Acknowledgments I wish to thank Charles Barth and the Mariner ultraviolet spectroscopy team for making available their Lyman α data. The many useful discussions with D. J. Strickland concerning this study are gratefully acknowledged. Charles Barth provided support for this work through the National Aeronautics and Space Administration under NASA contract NGL-06-003-052.

* * *

The Editor thanks J. C. McConnell and B. A. Tinsley for their assistance in evaluating this paper.

References

Anderson, D. E., Jr., and C. W. Hord, Mariner 6 and 7 ultraviolet spectrometer experiment: Analysis of hydrogen Lyman alpha data, *J. Geophys. Res.*, *76*, 6666, 1971.

Anderson, D. E., Jr., and C. W. Hord, Correction, *J. Geophys. Res.*, *77*, 5638, 1972.

Barth, C. A., W. G. Fastie, C. W. Hord, J. B. Pearce, K. K. Kelly, A I. Stewart, G. E. Thomas, G. P. Anderson, and O. F. Raper, Mariner 6: Ultraviolet spectrum of Mars upper atmosphere, *Science*, *165*, 1004, 1969.

Barth, C. A., C. W. Hord, J. B. Pearce, K. K. Kelly, G. P. Anderson, and A. I. Stewart, Mariner 6 and 7 ultraviolet spectrometer experiment: Upper atmosphere data, *J. Geophys. Res.*, *76*, 2213, 1971.

Barth, C. A., C. W. Hord, A. I. Stewart, and A. L. Lane, Mariner 9 ultraviolet spectrometer experiment: Initial results, *Science*, *175*, 309, 1972*a*.

Barth, C. A., A. I. Stewart, C. W. Hord, and A. L. Lane, Mariner 9 ultraviolet spectrometer experiment: Mars airglow spectroscopy and variations in Lyman alpha, *Icarus*, *17*, 457, 1972*b*.

Bohlin, R. C., Mariner 9 ultraviolet experiment: Measurements of the Lyman-alpha sky background, *Astron. Astrophys.*, *28*, 323, 1973.

Bruner, E. C., Jr., and W. A. Rense, Rocket observations of profiles of solar ultraviolet emission lines, *Astrophys. J.*, *157*, 417, 1969.

Colegrove, F. D., F. S. Johnson, and W. B. Hanson, Atmospheric composition in the lower thermosphere, *J. Geophys. Res.*, *71*, 2227, 1966.

Hunten, D. M., and M. B. McElroy, Production and escape of hydrogen on Mars, *J. Geophys. Res.*, *75*, 5989, 1970.

Kliore, A. J., D. L. Cain, G. Fjelbo, B. L. Seidel, and S. I. Rasool, Mariner 9 *S*-band Martian occultation experiment: Initial results on the atmosphere and topography of Mars, *Science*, *175*, 313, 1972.

McElroy, M. B., and J. C. McConnell, Dissociation of CO_2 in the Martian atmosphere, *J. Atmos. Sci.*, *28*, 879, 1971.

Pearce, J. B., K. A. Gause, E. F. Mackey, K. K. Kelly, W. G. Fastie, and C. A. Barth, The Mariner 6 and 7 ultraviolet spectrometers, *Appl. Opt.*, *10*, 805, 1971.

Stewart, A. I., Mariner 6 and 7 ultraviolet spectrometer experiment: Implications of CO_2^+, CO, and O airglow, *J. Geophys. Res.*, *77*, 54, 1972.

Stewart, A. I., C. A. Barth, C. W. Hord, and A. L. Lane, Mariner 9 ultraviolet spectrometer experiment: Structure of Mars upper atmosphere, *Icarus*, *17*, 469, 1972.

Strickland, D. J., and D. E. Anderson, Jr., Theoretical emergent Lyman α intensities from Mars, *J. Geophys. Res.*, *78*, 6491, 1973.

Strickland, D. J., A. I. Stewart, C. A. Barth, C. W. Hord, and A. L. Lane, Mariner 9 ultraviolet spectrometer experiment: Mars atomic oxygen 1304-Å emission, *J. Geophys. Res.*, *78*, 4547, 1973.

Thomas, G. E., and R. F. Krassa, Ogo-5 measurements of the Lyman alpha sky background, *Astron. Astrophys.*, *11*, 218, 1971.

(Received August 9, 1973;
accepted January 4, 1974.)